ChemPubSoc Europe

DOI: 10.1002/cctc.201600860

CHEMCATCHEM Full Papers

Effect of Feedstock and Catalyst Impurities on the Methanol-to-Olefin Reaction over H-SAPO-34

Charlotte Vogt, Bert M. Weckhuysen,* and Javier Ruiz-Martínez[a]

Operando UV/Vis spectroscopy with on-line mass spectrometry was used to study the effect of different types of impurities on the hydrocarbon pool species and the activity of H-SAPO-34 as a methanol-to-olefins (MTO) catalyst. Successive reaction cycles with different purity feedstocks were studied, with an intermittent regeneration step. The combined study of two distinct impurity types (i.e., feed and internal impurities) leads to new insights into MTO catalyst activation and deactivation mechanisms. In the presence of low amounts of feed impurities, the induction and active periods of the process are prolonged. Feed impurities are thus beneficial in the formation of the initial hydrocarbon pool, but also aid in the unwanted formation of deactivating coke species by a separate, competing mechanism favoring coke species over olefins. Further, feedstock impurities strongly influence the location of coke deposits, and thus influence the deactivation mechanism, whereas a study of the organic impurities retained after calcination reveals that these species are less relevant for catalyst activity and function as "seeds" for coke formation only.

Introduction

Depletion of fossil fuel reserves and fluctuating crude oil prices have triggered an increased interest in the utilization of chemical processes with crude oil alternative feedstocks, such as coal, natural gas, and biomass. The catalytic conversion of (mixtures of) alcohols, derived from these crude oil alternative feedstocks, into a range of desired hydrocarbons is one of these promising technologies. Alcohols, such as methanol and ethanol, derived from synthesis gas and biomass can selectively be converted into lower olefins, such as ethylene and propylene, which are key building blocks for, for example, the polymer industry.[1–3] Driven by these possibilities, methanol-to-olefins (MTO) plants are emerging throughout, for example, Asia. China in particular, where the sheer abundance of coal motivates the construction of plants with conversion capacities of up to 600 kiloton.[4] Solid acids can be used to catalyze this reaction. H-SAPO-34 has prevailed over the original MTO catalyst, H-ZSM-5, as one of the most suitable catalysts for this catalytic reaction. Its particular pore size and shape make it highly selective towards the desired light olefins. This progress improved the MTO process economic viability in industry.[4] Unfortunately, what makes this catalyst so uniquely for the production of light olefins also bolsters rapid deactivation as small-pore H-SAPO-34 easily becomes diffusion-limited or blocked. Over time, great efforts have been made towards decreasing deactivation rates and increasing catalyst activity. Critical improvements have been made by modification of the catalyst crystal size and acidity; and an increased catalyst lifetime is reported for smaller crystal size and lower acidity.[5–11]

The MTO process is very dynamic and its mechanism is still not fully understood. The literature describes two main mechanisms for methanol-to-hydrocarbon (MTH) reactions over catalysts, such as H-SAPO-34; the paring mechanism and the side-chain methylation route. Both mechanisms rely on a so-called hydrocarbon pool (HCP) to form olefins. The autocatalytic HCP mechanism has gained unanimous acceptance.[12–15] According to this mechanism, methanol reacts onto a pool of organic intermediates to yield a wide range of hydrocarbons.[16] Active species in the HCP are poly-methyl-substituted benzeniums,[17] and deactivation is likely caused primarily by coke deposition.[18–29]

The formation of the hydrocarbon pool has been a source of significant debate by researchers and the literature is imbued with diverse and often conflicting theories resulting from a wide array of experimental analytical approaches.[26–39] The formation of the initial C–C bond during the induction period is at the base of this debate.[2a–c,34] Very recently, Sautet et al. reported that γ-Al_2O_3 activated at high temperature (973 K) is able to activate dimethyl ether via oxonium ions to form the first C–C bond.[35] However, several research groups have reported that the addition of impurities to the feedstock yields a co-catalytic or promoting effect and decreases the induction period of the MTH reaction; Mole et al. present this promoting effect after the addition of toluene to the methanol reagent in

[a] C. Vogt, Prof. Dr. B. M. Weckhuysen, Dr. J. Ruiz-Martínez
Inorganic Chemistry and Catalysis Group,
Debye Institute for Nanomaterials Science
Utrecht University
Universiteitsweg 99
3584 CG Utrecht (The Netherlands)
E-mail: b.m.weckhuysen@uu.nl

Supporting information for this article can be found under: http://dx.doi.org/10.1002/cctc.201600860.

a ZSM-5 catalyst.[40] Haw et al. followed this approach by suggesting that the initial bond formation proceeds not through a direct route, but rather by the presence of organic impurities.[41] External "impurities", such as toluene, ethanol, and acetone, are proven to have an effect on the MTO process.[3,41–43] The complexity of the MTO reaction undoubtedly allows the (simultaneous) existence of both a direct and an indirect mechanism, in which the prevailing mechanism is dependent on the system and the tools used to observe it.

Impurities are particularly relevant for the MTO reaction for two reasons. First, this crude oil alternative pathway to olefins will likely be fed by methanol made from biomass, coal, or natural gas. This methanol is reported to have up to 5–7% impurities, consisting mainly of ethanol and acetone.[3] As these compounds already contain a C–C bond, they might spark the hydrocarbon pool, but they may also affect other simultaneously occurring mechanisms, such as deactivation. Second, as previously mentioned, H-SAPO-34 is prone to rapid deactivation owing to its small pore size. For this reason, catalyst regeneration is practically necessary, but is also likely to leave some organic impurities.[42]

We define impurities to stem from two different sources; the aforementioned external impurities from, for example, organic impurities in the methanol feed, and internal or intrinsic impurities, which are carbon deposits that are retained in the zeolite material originating from any remaining template organics or a catalyst regeneration procedure.[41] It is worth noting that impurities remaining after calcination to remove templates might differ in nature from those after regeneration as detemplation could leave the catalyst with (stable) N-containing coke.

The extensive number of publications dealing with the effect of feedstock impurities[41–45] is in contrast with the lack of fundamental understanding on the influence of internal impurities (i.e., hydrocarbon deposits) in reactions with zeolites or zeotypes. To the best of our knowledge, there are no studies providing detailed information about their effect on the zeolite's catalytic performance and the role of these impurities on the origin of the first active HCP species.

More details about the nature and the effect of different types of impurities on catalytic performance are necessary and could prove to have practical relevance as an industrial MTO reaction is typically exposed to these impurities. In previous studies, our group has provided experimental evidence for the formation of distinct zeolite-occluded hydrocarbon species upon detemplation.[46,47] Karwacki et al. studied the template decomposition process in large ZSM-5 crystals by using in situ fluorescence microscopy and reported increasingly larger (conjugated) aromatic molecules with increasing temperatures. These larger coke-like derivatives are more resistant to thermal decomposition.[46] Qian et al. studied the detemplation of H-SAPO-34 by use of (UV/Vis) micro-spectroscopy and found evidence for methyl-substituted benzenium cations remaining in the zeolite crystal after detemplation.[47] Compellingly, poly-methyl-substituted benzenes are believed to be active species in the HCP, which may imply that these types of impurities are a potential origin for the formation of the HCP.[48,49] In other words, organic templates may leave species after thermal detemplation with similar chemistry to post-regeneration, which is likely to affect the (age of the) HCP in a similar way. These findings have sparked our interest to understand the effect of a regeneration treatment on catalytic performance, as this equally relevant step in MTO reaction chemistry has gained significantly less attention.

The current study focuses on the effect of two types of impurities on the performance of H-SAPO-34 as an active MTO catalyst material; external (i.e., feedstock) and internal (i.e., coke deposits after catalyst regeneration). By studying the interplay between these two impurity types in tandem, their chemistry and effect on catalyst performance is evaluated. This will be done by studying the effect of different impurity types, as well as retained impurities after a regeneration procedure by operando UV/Vis spectroscopy and on-line mass spectrometry.

Results and Discussion

Combined operando UV/Vis spectroscopy and on-line mass spectrometry

The multifaceted data obtained with our operando set-up allowed us to further understand the effect of the different purity feedstocks at the molecular level by comparing catalyst activity (using mass spectrometry) with the nature of species formed inside the catalyst (using time-resolved UV/Vis spectroscopy). Figures 1–3 depict the complete set of results that have been obtained with this operando UV/Vis spectroscopy/mass spectrometry setup for the three different methanol purities, that is; methanol (E), (A), and (U), respectively. Figures 1a, 2a, and 3a show the on-line mass spectrometry profiles for methanol, propylene, and DME during the catalytic test. These operando data link the catalyst activity to the formation of species inside the catalyst during an MTO reaction cycle, regeneration, and a subsequent MTO reaction cycle for the three methanol purities.

In a typical experiment, the H-SAPO-34 catalyst wafer was placed on the heating stage of the custom-built cell and activated before every reaction. A range of different feedstock purities (listed in Table 1; indicated by (E): methanol with 5% ethanol; (A): analytical grade methanol with 270 ppm acetone and ethanol impurities; and (U): ultra-pure methanol with 49 ppm

Table 1. Overview of the methanol feedstocks explored in this work, including the main impurities.

Feedstock purity and related feedstock abbreviation	Amount of impurities [ppm]	Main impurities	Kinetic diameter [Å]	Other impurities[a]
Ultra-pure (U)	49	acetone	3.1	–
Analytical-grade (A)	270	acetone	3.1	ethanol
Ethanol in methanol (E)	$\geq$50 000	ethanol	3.8	acetone

[a] Other impurities $<$5% of total impurities.

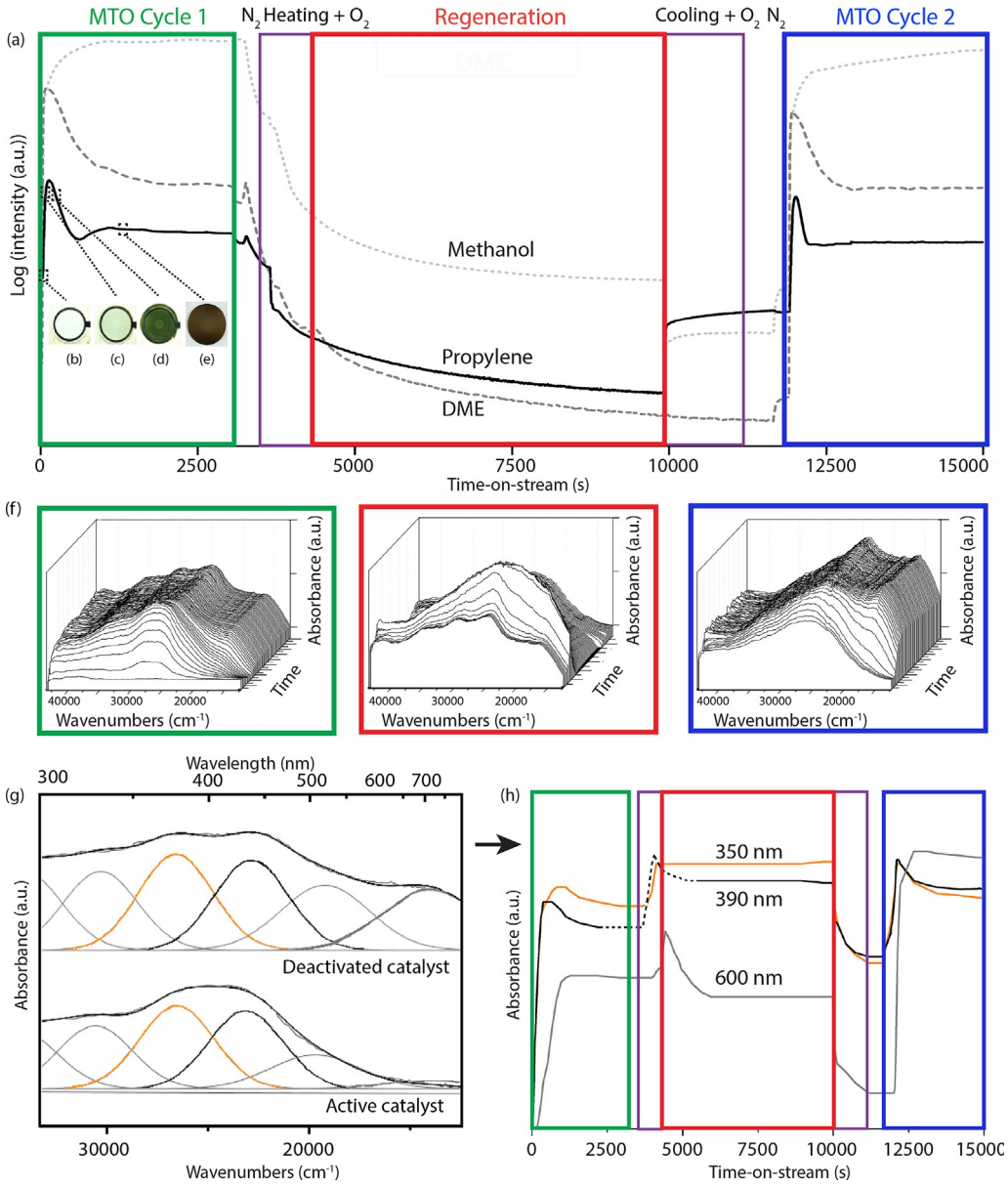

Figure 1. (a) Mass spectrometry profile of a methanol-to-olefins (MTO) experiment over a H-SAPO-34 catalyst performed at 623 K with a regeneration step at 823 K and methanol (E) (i.e., 5 wt% ethanol in methanol) as feedstock. For MTO cycle 1, the methanol flow is introduced at 623 K. Subsequently, the catalyst pellet was flushed with N_2.Regeneration starts with the introduction of an O_2 flow and temperature increase to 823 K. The pellet was then flushed once more and the temperature was decreased back to the initial reaction temperature of 623 K. After this regeneration step, a second MTO cycle was started. (b–f) Photographs representative of a typical catalyst wafer (b) before reaction, (c) in the active period, (d) deactivating, and (e) deactivated. (f) Time-resolved operando UV/Vis spectra of the catalyst pellet during MTO cycle 1, regeneration, and MTO cycle 2. (g) A selection of operando UV/Vis spectra during the active and deactivating periods of the first MTO cycle (active species at 350 nm and 390 nm, orange and black lines, respectively, and deactivating species at around 600 nm, dark grey line). (h) Intensity profiles of the absorption bands at 350, 390, and 600 nm, representative for the active and deactivating species, as obtained after deconvoluting the collected operando UV/Vis spectra. The dotted line indicates a spectral shift (only indicated in the active period) from 390 to 400 nm. More information about the deconvolution procedure can be found in the Supporting Information (§S.1).

acetone impurities, further discussed in the Experimental Section, and listed in Table 1) was fed through a saturator using N_2 as a carrier gas, as mentioned previously. The most abundant mass of propylene, $m/z = 41$, has been chosen as a descriptive mass for olefin formation. Both ethylene and propylene formation follow the same trend in the mass spectrometry results and the choice for propylene was arbitrary. Quantitative analysis showed slightly more ethylene over propylene, with DME as the only side product detected by gas chromatography.

Propylene formation begins when the propylene slope changes, as for all displayed species. This marks the transition between the induction period and the active period, typically lasting tens of seconds (as summarized and displayed in a graphical overview in Figure 4). During the first MTO cycle, methanol is introduced at 623 K; subsequently the pellet was

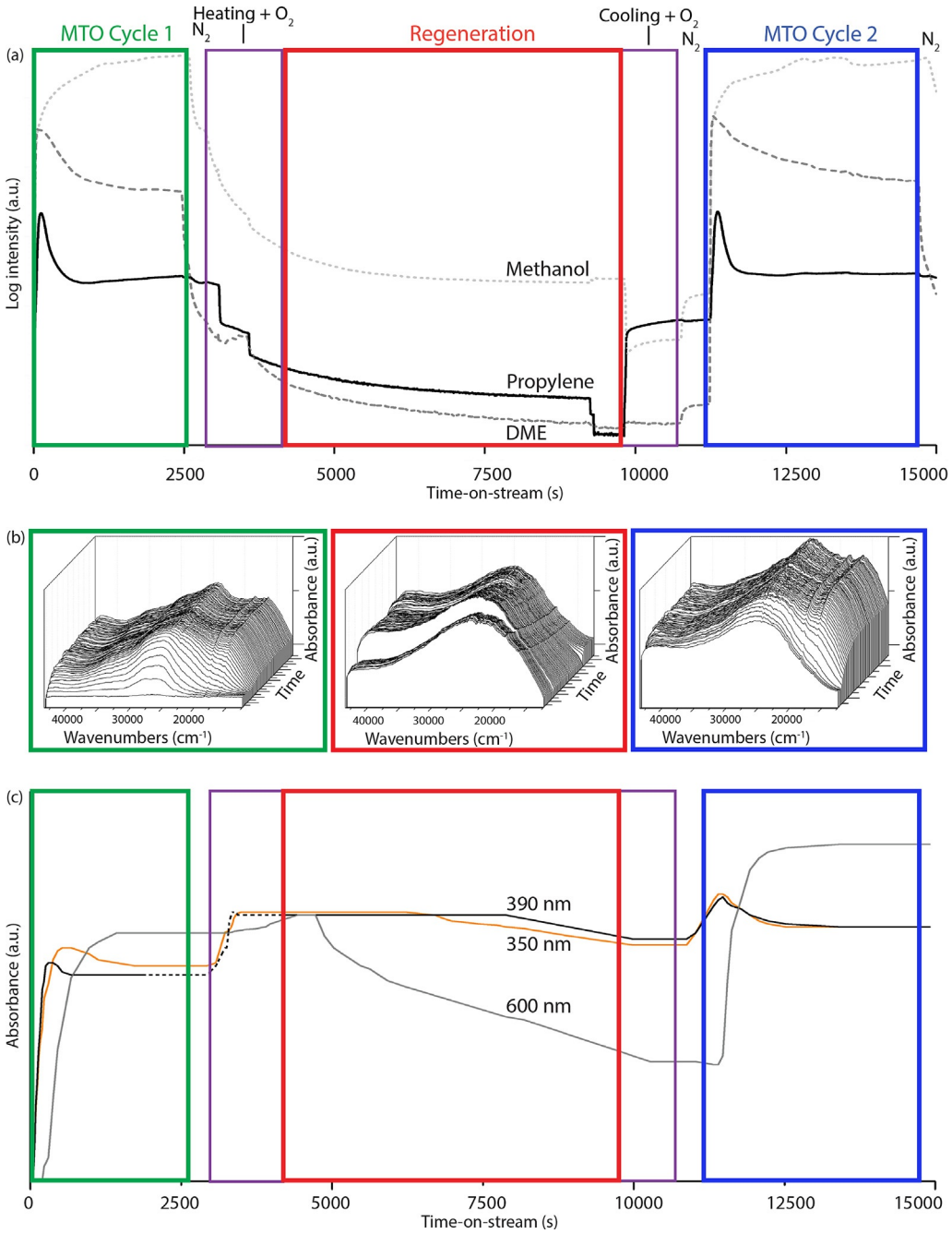

Figure 2. Operando UV/Vis spectroscopy measurements of a methanol-to-olefins (MTO) experiment over a H-SAPO-34 catalyst with methanol (A) (i.e., analytical grade methanol) as a feedstock. (a) Mass spectrometry profile of an MTO experiment performed at 623 K, with a regeneration step at 823 K. For MTO cycle 1, the methanol flow is introduced at 623 K. Subsequently, the pellet was flushed with N_2 and regeneration is initiated by the introduction of an O_2 flow and temperature increase to 823 K. The pellet was then flushed once more and the temperature was decreased back to the reaction temperature of 623 K. After this regeneration step, a second MTO cycle was started. (b) Time-resolved UV/Vis spectra of the catalyst pellet during MTO cycle 1, regeneration, and MTO cycle 2. Notably, a vertical shift of spectra occurs for the regeneration period. This is an artifact (which is corrected for in the deconvoluted data) and is most likely caused by the proximity of the UV/Vis probe to the non-insulated reaction cell at high regeneration temperatures. (c) Evolution of the 350, 390, and 600 nm deconvoluted UV/Vis bands. The dotted line indicates a spectral shift (only indicated in the active period) from 390 to 400 nm. More information about the deconvolution of the UV/Vis spectra can be found in the Supporting Information (§S.1).

flushed with N_2 to reduce the amount of gaseous product in the catalyst. Deactivation (shown in Figures 1, 2, 3, and summarized in Figure 4) was determined by following the propylene profile by mass spectrometry, and is defined here as the point where olefin formation has decreased and appears steady. We rely here on a qualitative method to determine catalyst deactivation by looking at the drastic drop in olefin formation, such as observed in Figures 1, 2, and 3. This type of catalyst deactivation is expected for the deactivation of an eight-membered ring zeolite catalyst at our reaction condi-

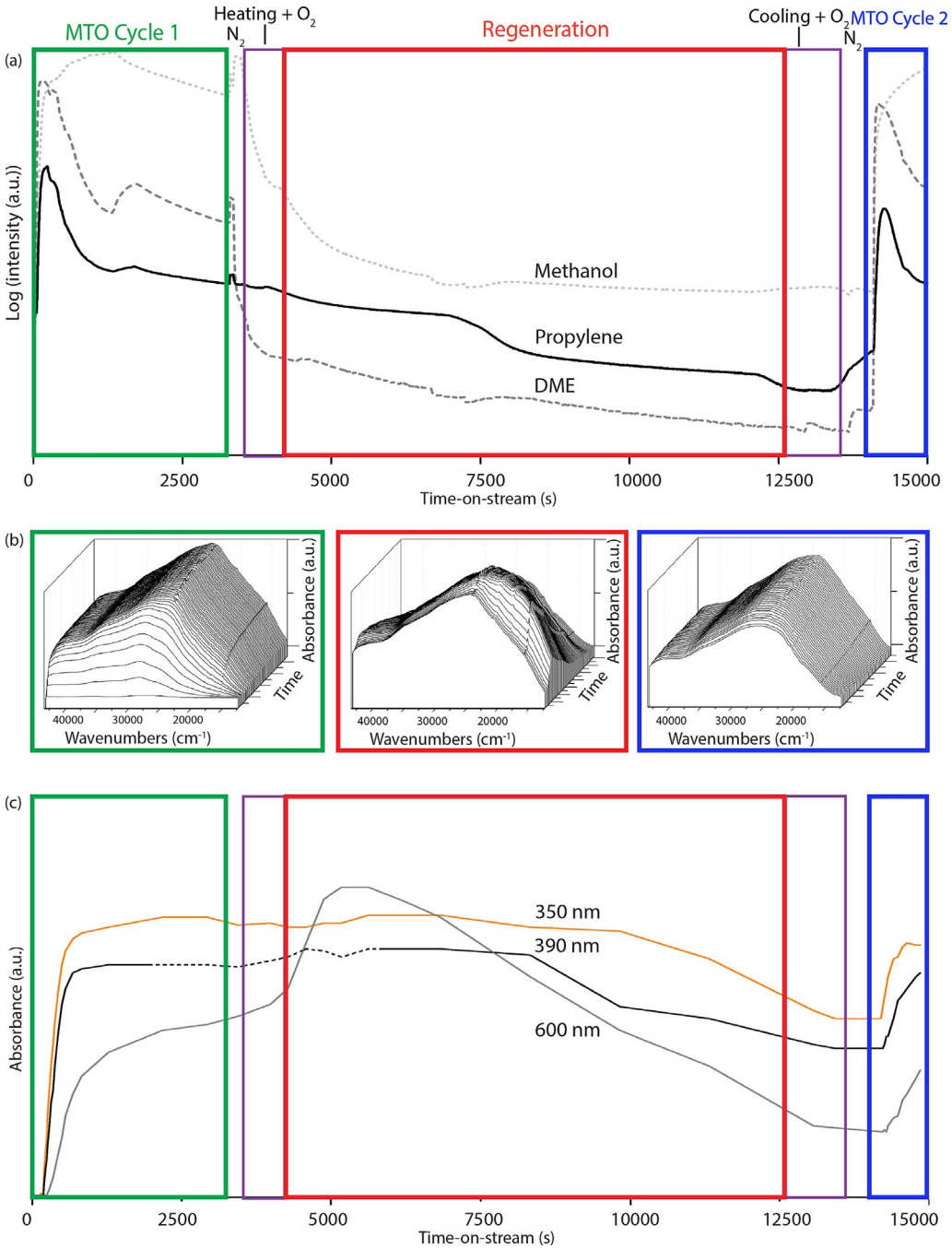

Figure 3. Operando UV/Vis spectroscopy measurements of a methanol-to-olefins (MTO) experiment over a H-SAPO-34 catalyst with methanol (U) (i.e., ultrapure methanol) as feedstock. (a) Mass spectrometry profile of an MTO experiment performed at 623 K with a regeneration step at 823 K. For MTO cycle 1, the methanol flow is introduced at 623 K. Subsequently, the pellet was flushed with N_2 and regeneration starts with the introduction of an O_2 flow and temperature increase to 823 K. The pellet was then flushed once more and temperature was decreased back to the reaction temperature of 623 K. After this regeneration step, a second MTO cycle was started. (b) Time-resolved UV/Vis spectra of the catalyst pellet during MTO cycle 1, regeneration, and MTO cycle 2. (c) Evolution of the 350, 390 and 600 nm deconvoluted UV/Vis bands. The dotted line indicates a spectral shift (only indicated in the active period) from 390 to 400 nm. More information about the deconvolution of the UV/Vis spectra can be found in the Supporting Information (§S.1).

tions.[50] Furthermore, visible inspection of the catalyst wafer during reaction suggests deactivation by poly-aromatics (Figure 1 b–f).

After catalyst deactivation, the pellet (at this point colored dark brown to black) was flushed with N_2 and the temperature was increased to 823 K in an O_2 flow for catalyst regeneration. Subsequent to this regeneration procedure, the catalyst pellet was flushed a second time with N_2 and brought back to the reaction temperature, after which a second MTO cycle was initiated. Finally, methanol was introduced once more as the second MTO cycle commences. Figure 1 a shows the on-line mass spectrometry profiles for methanol, propylene, and DME

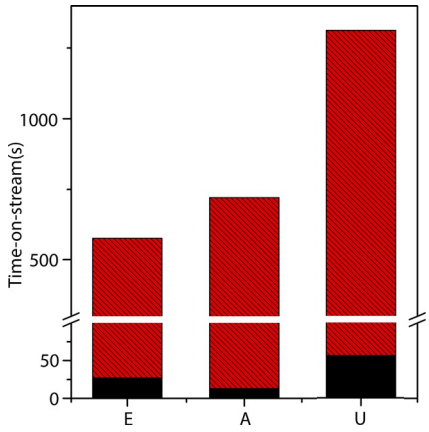

Figure 4. An overview of the induction periods (black) and active periods (red) for the methanol-to-olefins (MTO) cycles conducted over a H-SAPO-34 catalyst at 623 K with methanol feedstock containing different degrees of impurities: (E), (A), and (U). The induction period is defined as the time up to the start of the formation of propylene.

of the experiment with methanol (E) as feedstock. Similar data have been obtained for methanol (A) and (U) as feedstock and the results can be found in Figures 2a and 3a.

The vertical lines delineate the different steps of the experiment; that is, first MTO cycle, N_2 flushing, regeneration in O_2; N_2 flushing; and second MTO cycle. Figure 1f displays the time-resolved operando UV/Vis spectra for MTO cycle 1, regeneration, and MTO cycle 2 (and Figures 2b, 3b show the same for methanol (A) and (U) feedstocks, respectively).

As the collected operando UV/Vis spectra for each MTO experiment are broad and contain several overlapping absorption bands, a systematic deconvolution procedure was applied to further analyze the UV/Vis spectra. A detailed explanation and overview of the choices made for the selection of the Gaussian bands can be found in the Supporting Information (§S.1). Figure 1h shows the deconvolution of two separate UV/Vis spectra; of the active and deactivated catalyst material during MTO cycle 1 for exemplary purposes. Two regions of UV/Vis absorption bands in all spectra in Figures 1f, 2b, and 3b are apparent at first glance; these are crucial for the understanding of the interplay of species in the activation and deactivation of H-SAPO-34 as a catalyst in the MTO reaction. These two regions are characterized by an absorption below 400 nm (25000 cm^{-1}) and a broad absorption at 600–700 nm (16600–14300 cm^{-1}); both have previously been identified as active and deactivating hydrocarbon species, respectively.[22,51,52] Notably, all hydrocarbon species could, in principle, contribute in the conversion of methanol in the initial stage of the MTO process. For this reason, the terms used to describe these species are not absolute, but rather an indication of their main role in the described MTO experiments. An overview of the bands and their assignments can be found in Table 2, based on this work, previous work by our group, as well as literature findings.[26,45,49,52] We do not imply the divisions between the different spectral regions are in reality as strict as denoted in this table owing to the high number of species that absorb within the range of the UV/Visible spectrum, which also play a role in the hydrocarbon pool mechanism. However, this division will assist in confidently assigning bands to certain (types of) hydrocarbon species.

Table 2. Assignment of the operando UV/Vis bands used in this work.

Wavelength [nm]	Wavenumber [cm^{-1}]	Assignment
270	37000	neutral benzenes* [45,57]
300	33000–34000	monoenylic carbenium ions* [45,57]
325–330	29500–30500	dienylic carbenium ions [57]
350–365	28000–30000	less-alkylated benzenes [49]
390	25000–26000	poly-alkylated benzenes
400	25000	non-protonated mono- or dicyclic aromatics
600	16000–17000	polycyclic aromatics (coke)* [45,57]

An asterisk (*) indicates the bands have been confirmed by previous work.

The formation of the absorption bands at around 600–700 nm only proceeds towards the end of the reaction (as the spectrum for the deactivated catalyst in Figure 1h clearly indicates), when olefin formation has started to decrease. This indicates that this spectral region is descriptive for the presence of larger poly-aromatic systems or coke-like species, which may block the pores and thus hinder molecules from reaching the catalytically active Brønsted acid sites within the nanocages and therefore deactivate the catalyst material.[20,24,49] These hydrocarbon species might also be aged hydrocarbon pool species that have reacted and subsequently are no longer active in the pool and do not yield olefins. The spectral region below 400 nm is of particular interest in the active period of the MTO process. The evolution of these absorption bands suggests that some of these species have an active role in the production of olefins. Highly poly-methylated benzenes have been determined to be active species in the formation of olefins and have been suggested to absorb light between 390–400 nm.[24,57–61] More specifically, some characterization studies suggest that the more active, highly methylated benzenes absorb light around 390 nm, whereas the non-active, less-methylated naphthalenic species absorb light near 400 nm.[17,20,49,61] This spectral shift from 390 to 400 nm is also observed in the data shown in Figure 1h, indicated by a dotted line. Recent work suggests that the UV/Vis band absorbing at around 350 nm corresponds to low-methylated benzenes and these species can take part in the MTO reaction through (de-)methylation, and are hence either active species or the direct result of MTO activity.[45a]

The evolution of the different UV/Vis absorption bands of active and deactivating species can be followed by plotting their intensities, as obtained by deconvolution, against time-on-stream. This procedure is applied and plotted in Figure 1h for the experiment with methanol (E) as feedstock (and Figures 2c, and 3c for methanol (A) and (U), respectively). Henceforth, we will examine the role of these active and deactivating species with the aid of the evolution of these absorption

bands descriptive for active and deactivating species; not only during reaction, but also regeneration.

The contribution of different purity feedstocks to overall catalyst activity can be seen in Figures 1a, 2a, and 3a. At first glance, we can clearly see a difference in the active periods of the reactions fed with different feedstocks. That is, methanol feedstock (U) containing very few impurities has a much longer active period than methanol (E) containing a relatively high concentration of impurities. Furthermore, we see that the production of intermediate dimethyl ether (DME) follows the trend of olefin production for all three feedstock purities. These results are summarized in Figure 4. Figure 4 depicts the *induction* periods (black) and *active* periods (red) of catalysts deactivated by the three different methanol purities as measured by on-line mass spectrometry. Feedstock impurities clearly have an effect on the induction period as previously reported.[40,61–64] The results summarized in Figure 4 show that methanol feedstock (U), containing very few impurities, has the longest induction and active periods. In general, it can be said that fewer gas-phase impurities lead to longer induction and active periods. However, the elongated induction period for methanol (E) with respect to methanol (A), containing less impurities, also suggests a competing pathway for ethanol-to-olefins conversion, which was previously noted by our group.[43] That is, the ethanol-to-olefins (ETO) process leads to the selective formation of aromatics, or coke deposits, over olefins.[49,50,2] Feedstock impurities are beneficial in the initial formation of the hydrocarbon pool, but they also aid in the (unwanted) formation of coke species.

An analysis of catalyst regeneration brings valuable insights into the deactivation mechanism under different feedstocks. Figure 5 shows the time lapse before the first observed decrease in coke species from the onset of regeneration (as measured by operando UV/Vis spectroscopy, that is, the evolution of the broad absorption band at 600 nm) in black, as can also be seen in the plots of the deconvolutions of the time-resolved UV/Vis spectra (Figures 1h, 2c, and 3c). Additionally, the ratio of active versus coke species is shown, also measured by UV/Vis during the active period of the MTO reaction for each purity. As summarized in Figure 5, and shown in Figures 1, 2, and 3, the same MTO experiment fed by a more pure methanol feedstock (e.g., methanol (U)) is marked by a different evolution of the aromatic species during regeneration. Although the coke species for methanol (E) begin to burn off almost immediately, the species inside a catalyst deactivated by methanol (U) take longer to burn off. This is a first indication that a highly pure methanol feed deactivates a catalyst differently from a feedstock with (ethanol) impurities, and that the organic species in a catalyst deactivated by methanol (U) are less accessible to oxygen during regeneration. In the following results this assumption is given substantial ground.

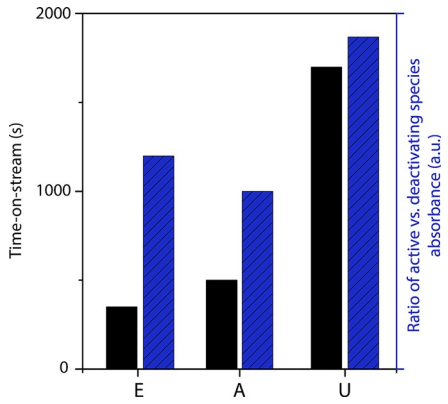

Figure 5. In black is the time indicative of the initial decrease of coke species from the onset of regeneration, as determined by deconvolution of time-resolved operando UV/Vis spectra. Blue bars are the ratios of UV/Vis absorption intensity between the active and deactivating, or less-active, species (350 and 390 nm, and 600 nm, respectively) for the (E), (A), and (U) feedstocks measured at maximum olefin formation.

This hypothesis also gives reason to the elongated active period observed for methanol containing fewer feedstock impurities. If methanol with impurities is fed, and increasingly large (poly-)aromatics form inside the catalyst cages, the pores are blocked from the outside-inwards as methanol can no longer diffuse inside the crystal where cages may still be free. Consequently, an MTO reaction fed with purer methanol uses the available active sites more efficiently.

This hypothesis is further supported by the ratios of active versus deactivating, or less-active, species as portrayed in Figure 5. The intensity ratio of the absorption bands representative for the active and deactivating species have been calculated by dividing the average absorbance of the UV/Vis absorption bands at around 350 and 390 nm by the absorbance of the 600 nm band, both determined at the point of maximum propylene formation in the MTO cycle.

The relatively high ratio of mono-aromatics versus poly-aromatics in methanol (U) suggests that deactivation occurs by filling the cages with mono-aromatics, which eventually causes diffusion limitations. Any incoming molecule is thus more likely to react with the outer surface mono-aromatics, which initiates the formation of poly-aromatics. Thus, a H-SAPO-34 catalyst fed with ultra-pure methanol is deactivated by the formation of a relatively thin layer of deactivating, or less-active poly-aromatics, but with a homogeneous distribution of active mono-aromatics. This homogeneous distribution of mono-aromatics is also the reason behind the longer activity if ultra-pure methanol is used.

The proposed deactivation mechanism, in which a homogeneous distribution of mono-aromatics causes deactivation for methanol (U), is supported by an initial gradual increase of the UV/Vis band descriptive for poly-aromatics during regeneration, suggesting that an increase in temperature causes mono-aromatics to agglomerate into coke species throughout the catalyst. This hypothesis is further illustrated by examining the UV/Vis spectra (Figure 6a, b) acquired during regeneration of a fully deactivated catalyst, and one that was still active. Figure 6a shows that in a fully deactivated catalyst, the broad band at around 600 nm ascribed to poly-aromatics decreases significantly whereas the active species retain their absorbance. Figure 6b illustrates that these active species, in an active catalyst, are still accessible and burn off much faster. In contrast,

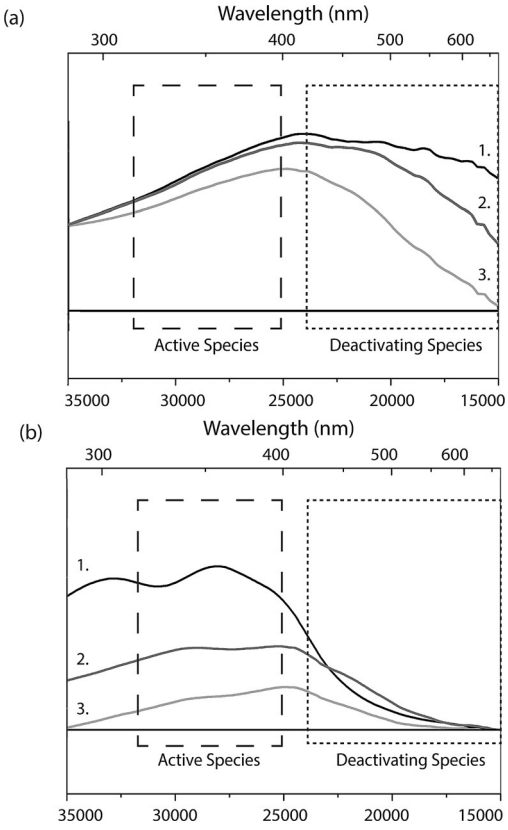

Figure 6. (a) Successive operando UV/Vis spectra (1, 2, 3) with increasing time-on-stream during the regeneration of a H-SAPO-34 sample after a - methanol-to-olefins (MTO) reaction with analytical grade methanol (A) after (a) complete deactivation and (b) a maximally active catalyst, (i.e., before deactivation of the catalyst has begun).

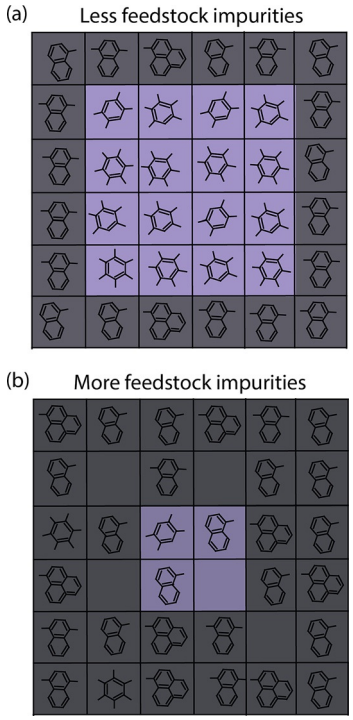

Figure 7. Schematic representation of the effect of feedstock impurities on catalyst deactivation. A H-SAPO-34 crystal deactivated with (a) methanol feedstock containing few impurities, such as methanol (U), containing 49 ppm acetone impurities, and (b) a methanol feedstock containing more feed impurities, such as methanol (E) with 5 wt% ethanol impurities. The darker color represents polyaromatics or coke, whereas the lighter color represents mono-aromatic or active species.

the lower ratio of mono-aromatics versus poly-aromatics in the methanol (A) and (E) feedstocks (Figure 5) suggests that catalyst deactivation likely occurs by pore blockage by poly-cyclic molecules throughout the H-SAPO-34 crystal. Figure 7 shows a schematic representation of the hypothesized effect of feedstock impurities on catalyst deactivation, which is in line with previous findings by our group.[43] This envisaged mechanism of deactivation is also supported by the relatively low absorbance of the active species (characterized by the absorption bands at 350 and 390 nm) if a methanol (E) feedstock is used compared with a methanol (U) feedstock (Figure 1 versus Figure 3, summarized in Figure 4). A first plausible explanation is that the impurities are directly converted into the coke species deactivating the catalyst material. The second possible mechanism relates to the reaction of the impurities with the active species leading to a more rapid formation of deactivating, or less-active species, compared with the methanol reagent.

These experiments with different purity feedstocks gave insight into the difference in deactivation mechanisms. Furthermore, despite the fact that the experiments discussed here are not spatially resolved, the integral nature of the data collected in these experiments is still able to show that the addition of external impurities allows one to influence the location of coke deposits inside the crystal. However, there are two main types of impurities in the MTO reaction; external, or feedstock impurities as previously discussed, and impurities that are internal to the crystal; that is, any remaining organics after, for example, a calcination procedure. The following paragraphs discuss the effect of coke deposition after regeneration on a subsequent MTO cycle, as investigated by operando spectroscopy and mass spectrometry.

The time-resolved UV/Vis spectra displayed in Figures 1 f, 2 b and 3 b show that the relatively common regeneration procedure that was applied in these experiments, that is, 2 h O_2 flow at 823 K, did not rid the catalyst of all organic species formed during the MTO reaction. The nature of the species inside the catalyst before and after regeneration was studied by dissolution of the catalyst wafers in hydrogen fluoride, and subsequent GC-MS analysis. A detailed explanation of these experiments, and the GC-MS profiles can be found in the Supporting Information (§S.2, Figure S1). The species found inside a deactivated catalyst consist of a diverse range of (alkylated) mono-, di-, and tri-aromatics; whereas for the regenerated catalyst, mainly oxygenated mono-aromatics were detected. By monitoring propylene formation for all three purity types, that is, methanol (E), (A), and (U), the induction and active periods were also determined before and after regeneration. Figure 8 a shows the outcome thereof for methanol (U), the trend of which is indicative for all three types of methanol feedstocks, that is, the induction period is longer after regeneration

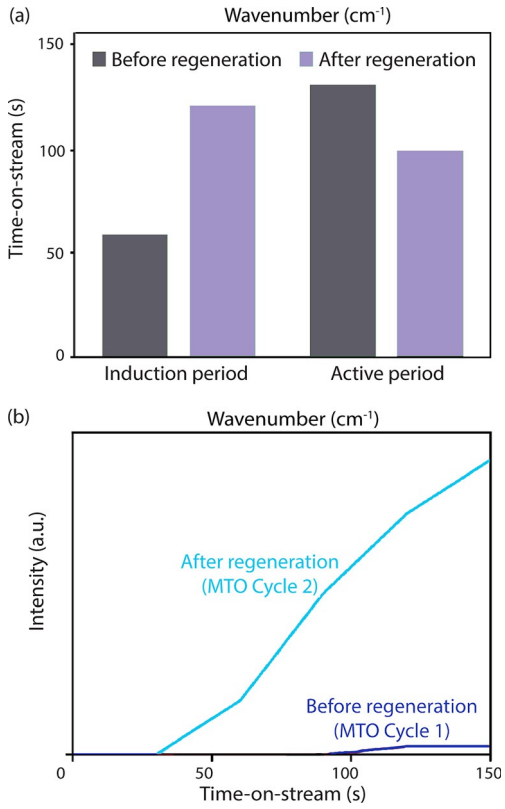

Figure 8. (a) Induction and active periods during the MTO reaction for the ultra-pure methanol (U) feedstock, before and after a regeneration procedure used to create intrinsic impurities. (b) Deconvoluted operando UV/Vis spectroscopy data during the MTO reaction of the active species (taking the representative absorption bands at around 350 and 390 nm) for ultra-pure methanol (U).

whereas the active period is shorter. Clearly, regeneration has an effect on catalyst lifetime. Deconvoluted UV/Vis data plotted with time-on-stream mark another compelling observation. The formation of UV/Vis absorption bands is faster if coke deposits are present, depicted in Figure 8b for methanol (U), but a similar trend was observed for each feedstock studied. The cumulative growth of the active species (bands at 350 and 390 nm) is shown in Figure 8b, which is representative for the growth of all species (including deactivating poly-aromatics) and indicative of the formation of a hydrocarbon pool. However, the fact that we also observe a longer induction period after regeneration (Figure 8a) suggests that the formation of these early species is, to a certain extent, independent of the formation of actual *active* hydrocarbon pool species. A faster increase in absorption occurs throughout the UV/Vis spectrum range in an MTO cycle after regeneration, as mentioned. The increase in formation of active species (350 and 390 nm), without the production of olefins however, may indicate that active species are formed but are blocked by larger poly-aromatics. Furthermore, non-active species may form that also absorb light in this region. The formation of olefins that are selectively transformed into deactivating aromatic species could also explain the longer induction period observed after regeneration. Aromatics that remain inside the crystal are consuming methanol, making species that are not active towards olefin formation. In other words, these retained aromatics after regeneration are "seeds" for the formation of coke species.

Our results show that catalyst regeneration has an effect on the activity of a second methanol-to-olefins cycle. Regeneration may also affect physical properties, for example, diffusivity or acidity of the zeolite crystal, which could lead to a similar effect on the activity. To thoroughly evaluate the effect of this single regeneration procedure, the induction periods after different severities of regeneration were examined. The results, displayed in Figure S2 (in the Supporting Information), showed that the induction period is always longer after regeneration on a partially and completely deactivated sample. Additionally, more severe regeneration of the catalyst (for 18 h, at 40:40 mL min^{-1} O_2/N_2) also results in a longer induction period. Ultra-pure methanol and results from this severe regeneration procedure show that almost no impurities in the catalyst will lead to an increased induction period, serving to bolster the hypothesis that impurities affect the stage of progression, or age, of the hydrocarbon pool. Thus, an optimum impurity profile for a minimal induction period most likely exists. These results also point out that diffusivity has not affected the induction period of these reactions.

Regeneration may also affect the acidity of a solid acid catalyst; it may alter the framework and cause a decrease in the number of acid sites and modify the average acid strength. In general, the hydrothermal conditions of the regeneration may cause a redistribution of silicon atoms into aggregates termed "silicon islands".[9,10] This will lead to the formation of silanol groups that can be detected with IR spectroscopy. A (partially) damaged catalyst could affect diffusion to the crystal and affect (effective) Brønsted acidity. However, no sign of the formation of silanol groups could be observed in the measured IR spectra (Figure S3 in the Supporting Information). In addition, a weakening of the acid strength would most likely result in a delay of the formation of aromatics, which is in disagreement with the results obtained with the presented reaction and regeneration procedure. Furthermore, the rate of formation of methoxy species inside the crystal, measured by monitoring the C–O stretching FTIR band at 940 cm^{-1}, is a measure for accessibility but also of acidity (Figure S4 in the Supporting Information).

With these results, we envisage an overall mechanism for the effect of the studied impurities in the MTO reaction over H-SAPO-34. In our proposal, if the catalyst is free of impurities —that is, before regeneration, or with a feedstock with few impurities— MTO active species are formed and will eventually deactivate the crystal with progressing catalyst lifetime. After regeneration of the catalyst, or with impurities in the feedstock, the H-SAPO-34 crystals will contain non-active aromatic species that easily create more deactivating species. This reaction is a competing reaction with the formation of olefins from the hydrocarbon pool, which is directly reflected in a longer induction period and shorter catalyst lifetime.

Conclusions

The use of operando UV/Vis spectroscopy with on-line mass spectrometry in a specially designed cell provided time-resolved information on the influence of different types of impurities on the methanol-to-olefins (MTO) reaction. This combined spectroscopic approach has proven to be useful from a practical angle, as impurities will inevitably be present during the MTO process. Two main groups of impurities are identified and assessed, that is, feed impurities (mainly ethanol and acetone) and impurities inside the catalyst after a calcination procedure, such as regeneration (i.e., poly-aromatics and coke).

The effect of methanol feedstock purity on catalyst activity, deactivation, and regeneration was examined with three different methanol purities. The results pointed out that, although feedstock impurities shorten the induction period, they also shorten the active period. A higher ratio of active versus deactivating, or less-active species, was also found to be present with fewer impurities, which led to the conclusion that feedstock impurities are beneficial in the formation of a hydrocarbon pool, but also promote the direct formation of deactivating coke species.

Additionally, operando UV/Vis spectroscopy data showed that methanol containing very few impurities gives a relatively high ratio of active versus coke species.

Time-resolved measurements during the regeneration of a catalyst deactivated by ultra-pure methanol showed that the deactivating species are burned off slowly and gradually. On the contrary, for a catalyst deactivated by methanol with a high amount of impurities, the same species burn off abruptly. These findings imply that impurities in the methanol feedstock cause catalyst deactivation by a layer of poly-aromatics, or coke, which block the rest of the crystal. On the other hand, methanol with few impurities deactivates by a more homogeneous distribution of aromatics effectively causing diffusion limitations, which then leads to a layer of poly-aromatics blocking the outside of the crystal. The main difference is thus the distribution of organic species throughout the crystal before it fully deactivates by a layer of poly-aromatics. Hence, changing the amount of feedstock impurities allows one to influence the location of coke species.

Performing a second MTO cycle with the studied regenerated H-SAPO-34 catalysts showed the influence of retained impurities after this calcination procedure. Although the induction period was always longer after regeneration, the formation of aromatics appeared sooner, which indicates that some impurities, remaining after, for example, calcination procedures, are seeds for the formation of larger coke species. This undesired reaction competes with the formation of the active hydrocarbon pool, and seems to be the preferred pathway.

Experimental Section

Combined operando UV/Vis spectroscopy with on-line mass spectrometry

Operando UV/Vis spectroscopy measurements were performed to study the hydrocarbon species trapped inside H-SAPO-34 cages, together with mass spectrometry to follow product formation during the MTO reaction. Time-resolved operando UV/Vis spectra were recorded to monitor the reaction and regeneration under different reaction conditions and with different feedstocks. The operando UV/Vis spectroscopy measurements were performed by using an Avantes Avalight-DH-S-BAL probe connected to an Avantes Avaspec 2048L spectrometer. Spectra were recorded every 15 s during each experiment. On-line analysis of the reaction products during the MTO reaction was obtained by a Pfeiffer Vacuum Omnistar mass spectrometer with a mass range of 5–55. The evolution of methanol, propylene, and dimethyl ether was tracked by monitoring the mass signals 31, 41, and 45, respectively.

Operando UV/Vis spectroscopy experiments were performed in a custom-built reaction cell, which is outlined in Figure S5 in the Supporting Information. The reaction cell was built with a very low dead volume to directly link the spectroscopic data with the catalytic performance of the material. The average residence time (τ) for a molecule in the gas phase in just the pipelines of the setup was 102 s and in the custom-built cell 125 s. The design of this cell is essential to this work as the it is the heart of the set-up. A comparison between the custom-built cell, and a commercial operando cell as well as more detailed information about the cell design and properties can be found in the Supporting Information (§S.4).

The H-SAPO-34 catalyst powders were pressed into pellets of approximately 16 mm diameter and around 0.1 mm thickness, weighing between 5–7 mg, by using a Laboratory Pellet Press and around 4 ton of pressure under vacuum. Before every reaction, the catalyst pellet was activated in oxygen (Linde 5.0). In this two-step activation, a 30 mL min^{-1} O_2 flow was introduced. In the first step, the temperature was ramped to 423 K at a rate of 5 K min^{-1}, and held there for 5 min, aiming to eliminate water. Then, the temperature was ramped to 723 K at a rate of 10 K min^{-1} to eliminate any other impurities in the zeolite material. After these two steps, the temperature was brought to the specific reaction temperature for that experiment and allowed to adjust to that temperature at a rate of 15 K min^{-1}. Then, methanol was fed through a saturator using a 10 mL min^{-1} flow of N_2 as a carrier gas, effectively containing approximately 13 % methanol.

Catalyst material and characterization

The catalyst used in the experiments described in this work is a commercial H-SAPO-34 material. The crystal size of this material was $\approx$4.3 μm (with standard deviation $\sigma = 0.9$) and the SiO_2:Al_2O_3 ratio used in the synthesis of the sample was 0.4, which can be translated theoretically into four acid sites per cage. Lower acidity and longer lifetimes are reported for lower silicon contents.[50,45a] The t-plot micropore volume of the sample under study is 0.25 cm^3 g^{-1}, whereas the mesopore volume is 0.2 cm^3 g^{-1}, calculated by using the Barrett–Joyner–Halenda (BJH) method of the material, argon physisorption isotherms, and the cumulative desorption pore volume in a range of 1–300 nm. Furthermore, the (relative) proton affinity measured by CO adsorption is 1179 kJ mol^{-1}, a characteristic value for an average of weak to medium strength acid sites.[45b] The Supporting Information shows an overview of these calculations for catalyst acidity characterization. NH_3 temper-

ature-programmed desorption (TPD) measurements displayed in Figure S7 (in the Supporting Information) revealed that, theoretically, the H-SAPO-34 sample has approximately 0.9 acid sites per cage and suggests that about 25% of the Si forms a Brønsted acid site. The CO adsorption FTIR spectra and NH_3-TPD profile can be found in the Supporting Information (§S.5).

Methanol feedstocks

It is important to mention that even high-purity methanol may contain enough organic impurities to create a hydrocarbon pool on a microporous solid acid catalyst. For example, "Acros Analysis Grade" methanol contains 270 ppm impurities of primarily acetone and ethanol. Acetone and ethanol are known precursors for the formation of cyclic (hydrocarbon pool) species.[45b] To investigate the effect of the extrinsic impurities in the feedstock, two methanol feedstocks with a different degree of impurities were prepared and compared with analytical grade methanol. An ultra-pure feedstock was prepared by following the procedure of Marcus et al.[53] "Acros Analysis Grade" methanol was fractionally distilled and kept in a glovebox to ensure no water or other impurities were adsorbed from the atmosphere. This methanol was then passed over a 10 cm column filled with dry molecular sieves (Linde type 4 Å) to remove any additional water. The methanol was subsequently passed over columns with pretreated Amberlyst 15 and Amberlyst 37, successively. This ultra-pure methanol contained 49 ppm of impurities (GC, FID detector) primarily consisting of 2,2-dimethoxyacetone. In addition, ultra-pure carrier gasses (Linde, 5.0) contain 1–10 ppm impurities, which might be a potential source of contamination. For this reason, a home-built gas trap with molecular sieves (Sigma–Aldrich, 5 Å) was installed to filter the O_2 and N_2 flows. The third methanol feedstock was created by adding 5 wt% of ethanol to ultra-purified methanol produced by the method described above, to observe the influence of this common impurity on the methanol feedstocks.[36]

The addition of ethanol to the feedstock may influence the reaction in a two-fold manner; the kinetic diameter of an ethanol molecule is closer to that of the micropores of H-SAPO-34, which makes diffusion slower, but recent work has also shown that the ethanol-to-olefins (ETO) process leads to the faster formation of poly-alkylated benzene carbocations and coke deposits.[49,50,54]

The type of impurities, concentrations, and gas methanol feedstock abbreviations are summarized in Table 1. All main impurities in the methanol feedstock fit inside the H-SAPO-34 micropores of around 0.38 nm in size assuming that the respective calculated diameters are the maximum size, and pore entry will proceed in a pore-parallel rather than pore-perpendicular manner.

Acknowledgments

J.R.M. acknowledges the Netherlands Organization for Scientific Research (NWO) for a VENI grant, and B.M.W. thanks NWO for a TOP research grant as well as a Gravitation program (Netherlands Center for Multiscale Catalytic Energy Conversion (MCEC)).

Keywords: catalyst deactivation · heterogeneous catalysis · methanol-to- olefins · operando spectroscopy · zeolites

[1] C. D. Chang, *Catal. Rev. Sci. Eng.* **1983**, *25*, 1 – 118.
[2] a) R. M. Dessau, R. B. Lapierre, *J. Catal.* **1982**, *78*, 136 – 141; b) W. Zatorski, S. Krzyzanowski, *Acta Phys. Chem.* **1977**, *24*, 347 – 352; c) C. N. Hamelinck, A. P. C. Faaij, *J. Power Sources* **2002**, *111*, 1 – 22.
[3] J. Q. Chen, A. Bozzano, B. Glover, T. Fugleerud, S. Kvisle, *Catal. Today* **2005**, *106*, 103 – 107.
[4] E. Jin, Y. Zhang, L. He, H. G. Harris, B. Teng, M. Fan, *Appl. Catal. A* **2014**, *476*, 158 – 174.
[5] B. M. Lok, C. A. Messina, R. L. Patton, R. T. Gajek, T. R. Cannan, E. M. Flanigen, *J. Am. Chem. Soc.* **1984**, *106*, 6092 – 6093.
[6] G. J. Yang, Y. X. Wei, S. T. Xu, J. R. Chen, J. Z. Li, Z. M. Li, J. H. Yu, R. R. Xu, *J. Phys. Chem. C* **2013**, *117*, 8214 – 8222.
[7] L. Wu, Z. Y. Liu, L. Xia, M. H. Qiu, X. Liu, H. J. Zhu, Y. H. Sun, *Chin. J. Catal.* **2013**, *34*, 348 – 356.
[8] Y. Cui, Q. Zhang, J. He, Y. Wang, F. Wei, *Particuology* **2013**, *11*, 468 – 474.
[9] Q. Wang, L. Wang, H. Wang, Z. X. Li, H. Wu, G. M. Li, X. P. Zhang, S. J. Zhang, *Asia Pac. J. Chem. Eng.* **2011**, *6*, 596 – 605.
[10] A. H. Zhang, S. L. Sun, Z. J. A. Komon, N. Osterwalder, S. Gadewar, P. Stoimenov, D. J. Auerbach, G. D. Stucky, E. W. McFarland, *Phys. Chem. Chem. Phys.* **2011**, *13*, 2550 – 2555.
[11] H. E. van der Bij, B. M. Weckhuysen, *Phys. Chem. Chem. Phys.* **2014**, *16*, 9892 – 9903.
[12] D. Lesthaeghe, V. Van Speybroeck, G. B. Marin, M. Waroquier, *Angew. Chem. Int. Ed.* **2006**, *45*, 1714 – 1719; *Angew. Chem.* **2006**, *118*, 1746 – 1751.
[13] D. M. Marcus, K. A. McLachlan, M. A. Wildman, J. O. Ehresmann, P. W. Kletnieks, J. F. Haw, *Angew. Chem. Int. Ed.* **2006**, *45*, 3133 – 3136; *Angew. Chem.* **2006**, *118*, 3205 – 3208.
[14] Y. D. Wang, C. M. Wang, H. X. Liu, Z. K. Xie, *Chin. J. Catal.* **2010**, *31*, 33 – 37.
[15] A. Comas-Vives, M. Valla, C. Coperét, P. Sautet, *ACS Cent. Sci.* **2015**, *1*, 313 – 319.
[16] I. M. S. Dahl, J. Kolboe, *J. Catal.* **1994**, *149*, 458 – 464.
[17] B. Arstad, S. Kolboe, *J. Am. Chem. Soc.* **2001**, *123*, 8137 – 8138.
[18] D. Chen, K. Moljord, T. Fuglerud, A. Holmen, *Microporous Mesoporous Mater.* **1999**, *29*, 191 – 203.
[19] K. Y. Lee, H. J. Chae, S. Y. Jeong, G. Seo, *Appl. Catal. A* **2009**, *369*, 60 – 66.
[20] N. Nishiyama, M. Kawaguchi, Y. Hirota, D. Van Vu, Y. Egashira, K. Ueyama, *Appl. Catal. A* **2009**, *362*, 193 – 199.
[21] W. Dai, G. Wu, L. Li, N. Guan, M. Hunger, *ACS Catal.* **2013**, *3*, 588 – 596.
[22] D. Mores, E. Stavitski, M. H. F. Kox, J. Kornatowski, U. Olsbye, B. M. Weckhuysen, *Chem. Eur. J.* **2008**, *14*, 11320 – 11327.
[23] D. Mores, J. Kornatowski, U. Olsbye, B. M. Weckhuysen, *Chem. Eur. J.* **2011**, *17*, 2874 – 2884.
[24] J. P. Hofmann, D. Mores, L. R. Aramburo, S. Teketel, M. Rohnke, J. Janek, U. Olsbye, B. M. Weckhuysen, *Chem. Eur. J.* **2013**, *19*, 8533 – 8542.
[25] F. Bleken, M. Bjørgen, L. Palumbo, S. Bordiga, S. Svelle, K.-P. Lillerud, U. Olsbye, *Top. Catal.* **2009**, *52*, 218 – 228.
[26] Q. Qian, C. Vogt, M. Mokhtar, A. M. Asiri, S. A. Al-Thabaiti, S. N. Basahel, J. Ruiz-Martínez, B. M. Weckhuysen, *ChemCatChem* **2014**, *6*, 3396 – 3408.
[27] U. Olsbye, S. Svelle, M. Bjørgen, P. Beato, T. V. W. Janssens, F. Joensen, S. Bordiga, K.-P. Lillerud, *Angew. Chem. Int. Ed.* **2012**, *51*, 5810 – 5831; *Angew. Chem.* **2012**, *124*, 5910 – 5933.
[28] V. Van Speybroeck, K. Hemelsoet, L. Joos, M. Waroquier, R. G. Bell, C. R. A. Catlow, *Chem. Soc. Rev.* **2015**, *44*, 7044 – 7111.
[29] E. T. C. Vogt, G. T. Whiting, A. D. Chowdhury, B. M. Weckhuysen, *Adv. Catal.* **2015**, *58*, 143 – 314.
[30] K. Hemelsoet, J. Van Der Mynsbrugge, K. De Wispelaere, M. Waroquier, V. Van Speybroeck, *ChemPhysChem* **2013**, *14*, 1526 – 1545.
[31] K. Hemelsoet, Q. Qian, T. De Meyer, K. De Wispelaere, B. De Sterck, B. M. Weckhuysen, M. Waroquier, V. Van Speybroeck, *Chem. Eur. J.* **2013**, *19*, 16595 – 16606.
[32] S. Svelle, M. Bjørgen, S. Kolboe, D. Kuck, M. Letzel, U. Olsbye, O. Sekiguchi, E. Uggerud, *Catal. Lett.* **2006**, *109*, 25 – 35.
[33] O. Sekiguchi, V. Meyer, M. C. Letzel, D. Kuck, E. Uggerud, *Eur. J. Mass Spectrom.* **2009**, *15*, 167 – 181.
[34] G. Guella, D. Ascenzi, P. Franceschi, P. Tosi, *Rapid Commun. Mass Spectrom.* **2007**, *21*, 3337 – 3344.
[35] A. Comas-Vives, M. Schwarzwälder, C. Copéret, P. Sautet, *J. Phys. Chem. C* **2015**, *119*, 7156 – 7163.
[36] W. Wang, A. Buchholz, M. Seiler, M. Hunger, *J. Am. Chem. Soc.* **2003**, *125*, 15260 – 15267.

[37] L. R. Aramburo, J. Ruiz-Martínez, L. Sommer, B. Arstad, R. Buitrago-Sierra, A. Sepfflveda-Escribano, H. W. Zandbergen, U. Olsbye, F. M. F. de Groot, B. M. Weckhuysen, *ChemCatChem* **2013**, *5*, 1386 – 1394.
[38] P. Tian, Y. Wei, M. Ye, Z. Liu, *ACS Catal.* **2015**, *5*, 1922 – 1938.
[39] M. Stöcker, *Microporous Mesoporous Mater.* **1999**, *29*, 3 – 48.
[40] T. Mole, J. Whiteside, *J. Catal.* **1983**, *82*, 261 – 266.
[41] W. Song, D. M. Marcus, H. Fu, J. O. Ehresmann, J. F. Haw, *J. Am. Chem. Soc.* **2002**, *124*, 3844 – 3845.
[42] C. M. Wang, Y. D. Wang, Z. K. Xie, *J. Catal.* **2013**, *301*, 8 – 19.
[43] Q. Qian, J. Ruiz-Martínez, M. Mokhtar, A. Asiri, M. Al-Tabaiti, H. E. van der Bij, B. M. Weckhuysen, *Chem. Eur. J.* **2013**, *19*, 11204 – 11215.
[44] Y. Jiang, W. Wang, R. Marthala, J. Huang, B. Sulikowski, M. Hunger, *J. Catal.* **2006**, *238*, 21 – 27.
[45] a) S. Wilson, P. Barger, *Microporous Mesoporous Mater.* **1999**, *29*, 117 – 126; b) L. Wu, E. J. M. Hensen, *Catal. Today* **2014**, *235*, 160 – 168.
[46] L. Karwacki, B. M. Weckhuysen, *Phys. Chem. Chem. Phys.* **2011**, *13*, 3681 – 3685.
[47] Q. Qian, D. Mores, J. Kornatowski, B. M. Weckhuysen, *Microporous Mesoporous Mater.* **2011**, *146*, 28 – 35.
[48] W. Dai, W. Kong, L. Li, G. Wu, N. Guan, N. Li, *ChemCatChem* **2010**, *2*, 1548 – 1551.
[49] E. Borodina, F. Meirer, I. Lezcano-Gonzalez, M. Mokhtar, A. M. Asiri, S. A. Al-Thabaiti, S. N. Basahel, J. Ruiz-Martínez, B. M. Weckhuysen, *ACS Catal.* **2015**, *5*, 992 – 1003.
[50] D. Chen, K. Moljord, A. Holmen, *Microporous Mesoporous Mater.* **2012**, *164*, 239 – 250.
[51] R. Nielsen, *Ullmann's Encyclopedia of Industrial Chemistry*, Wiley-VCH, Weinheim, **2010**.
[52] W. Song, J. B. Nicholas, J. F. Haw, *J. Phys. Chem. B* **2001**, *105*, 4317 – 4323.
[53] Y. Marcus, S. Glikberg, *Pure Appl. Chem.* **1985**, *57*, 855 – 864.
[54] Q. Qian, J. Ruiz-Martínez, M. Mokhtar, A. M. Asiri, S. A. Al-Thabati, S. N. Basahel, B. M. Weckhuysen, *ChemCatChem* **2014**, *6*, 772 – 783.
[55] M. Bjørgen, F. Bonino, S. Kolboe, K.-P. Lillerud, A. Zecchina, S. Bordiga, *J. Am. Chem. Soc.* **2003**, *125*, 15863 – 15868.
[56] Y. Jiang, J. Huang, R. Marthala, Y. S. Ooi, J. Weitkamp, M. Hunger, *Microporous Mesoporous Mater.* **2007**, *105*, 132 – 139.
[57] D. M. McCann, D. Lesthaeghe, P. W. Kletnieks, D. R. Guenther, M. J. Hayman, V. Van Speybroeck, M. Waroquier, J. F. Haw, *Angew. Chem. Int. Ed.* **2008**, *47*, 5179 – 5182; *Angew. Chem.* **2008**, *120*, 5257 – 5260.
[58] M. Bjørgen, S. Svelle, F. Joensen, J. Nerlov, S. Kolboe, F. Bonino, L. Palumbo, S. Bordiga, U. Olsbye, *J. Catal.* **2007**, *249*, 195 – 207.
[59] Y. Stepanenko, A. L. Sobolewski, A. Mordzinski, *J. Mol. Spectrosc.* **2005**, *233*, 15 – 22.
[60] A. Sassi, M. A. Wildman, H. J. Ahn, P. Prasad, J. B. Nicholas, J. F. Haw, *J. Phys. Chem. B* **2002**, *106*, 2294 – 2303.
[61] I. Kiricsi, H. Förster, G. Tasi, J. B. Nagy, *Chem. Rev.* **1999**, *99*, 2085 – 2114.
[62] J. F. Haw, W. G. Song, D. M. Marcus, J. B. Nicholas, *Acc. Chem. Res.* **2003**, *36*, 317 – 326.
[63] Z. Liu, Y. Qi, *Bull. Chin. Acad. Sci.* **2006**, *21*, 406 – 408.
[64] C. Yuan, Y. X. Wie, J. Li, S. Xu, J. Chen, Y. Zhou, Q. Wang, L. Xu, Z. Liu, *Chin. J. Catal.* **2012**, *33*, 367 – 374.

Received: July 14, 2016
Published online on November 29, 2016

